

## Linking of pedestrian spaces to optimize outdoor air ventilation and quality in tropical high-density urban areas

Yueyang He<sup>a,b,\*</sup>, Abel Tablada<sup>c</sup>, Ji-Yu Deng<sup>d</sup>, Yuan Shi<sup>e</sup>, Nyuk Hien Wong<sup>f</sup>, Edward Ng<sup>a,b,g</sup>

<sup>a</sup> Institute of Future Cities, The Chinese University of Hong Kong, Hong Kong, China

<sup>b</sup> Institute of Environment, Energy and Sustainability, The Chinese University of Hong Kong, Hong Kong, China

<sup>c</sup> Faculty of Architecture, Technological University of Havana J.A. Echeverría, Havana, Cuba

<sup>d</sup> School of Architecture and Urban Planning, Guangdong University of Technology, Guangzhou, China

<sup>e</sup> Department of Geography and Planning, University of Liverpool, Liverpool, UK

<sup>f</sup> Department of the Built Environment, College of Design and Engineering, National University of Singapore, Singapore

<sup>g</sup> School of Architecture, The Chinese University of Hong Kong, Hong Kong, China

### ARTICLE INFO

#### Keywords:

Open space  
Urban ventilation  
Pollutant dispersion  
Urban design  
CBD  
CFD

### ABSTRACT

Pedestrian spaces in cities allow a large number of outdoor activities. However, they are vulnerable to vehicular pollutants. This study aims to investigate how pedestrian spaces should be linked to optimize wind conditions and air quality in tropical cities. Numerical simulations are conducted to evaluate various upwind-to-downwind linking patterns in urban areas with three levels of high-density. The results suggest that wind velocity and pollutant concentration can be effectively optimized by adjusting their linking patterns even without compromising building density. However, wind velocity and pollutant concentration are not always inversely related. Key findings are achieved: 1) expanding pedestrian spaces particularly those at the upwind of a vehicle road introduces more prevailing wind which improves both air ventilation and quality in most scenarios; 2) offsetting pedestrian spaces at the upwind/downwind of a vehicle road generates more displacement (i.e., span-wise and vertical) flow which enhances pollutant dispersion; 3) diverging pedestrian spaces from the upwind to downwind restricts transmitting pollutants to the downwind; and 4) diversifying urban block configurations with more non-uniform linking patterns improves air quality but is less useful to wind conditions. A better-ventilated pedestrian environment is expected to encourage outdoor activities, promoting sustainable living styles and vibrant mixed-use urban developments.

### 1. Introduction

Tropical cities suffer from weak wind conditions for long periods of time annually. In high-density urban areas, the presence of compact built environment further weakens the wind conditions (He et al., 2021a; 2022a,b) and causes a series of relevant environmental issues, such as air pollution. Without adequate urban ventilation, air pollutants remain longer inside street canyons, hence leading to poorer air quality at pedestrian level (Buccolieri et al., 2010; Hang et al., 2009; Xie et al., 2005).

In Singapore, road vehicle is responsible for the major air pollutants in many urban areas (NEA, 2021). These transport-related

\* Corresponding author at: Institute of Future Cities, The Chinese University of Hong Kong, Hong Kong, China.  
E-mail address: [yueyanghe@cuhk.edu.hk](mailto:yueyanghe@cuhk.edu.hk) (Y. He).



**Fig. 1.** A vision to transform a high-density CBD into a vibrant mixed-use district: (a) narrow and conventional pedestrian spaces versus (b) expanded and vibrant pedestrian spaces (source: google earth).

pollutants contribute to ambient levels of air toxics which can cause a variety of health effects, such as neurological, cardiovascular, respiratory, reproductive and immune system damage (EPA, 2021a; Franco et al., 2013; Kampa and Castanas, 2008; Krzyzanowski et al., 2005; WHO, 2021; Zhang and Batterman, 2013). Some of these pollutants have been known or suspected as human carcinogens (EPA, 2021a) and associated with excess mortality (WHO, 2021). To indicate the levels of air quality, local agency has established the Pollutant Standards Index (NEA, 2014) which considers the classified concentration limits of six harmful air pollutants, including particulate matter (PM<sub>10</sub>), fine particulate matter (PM<sub>2.5</sub>), sulphur dioxide (SO<sub>2</sub>), carbon monoxide (CO), ozone (O<sub>3</sub>) and nitrogen dioxide (NO<sub>2</sub>). Along with the index, long-term targets have been set to satisfy the international criteria recommended by the “National ambient air quality standards” (EPA, 2021b) of the United States and “World Health Organization (WHO) air quality guidelines” (WHO, 2016). With these efforts and implemented measures, Singapore enjoys significantly better air quality than many cities in Asia on an annual average basis (NEA, 2021). However, those high-density urban areas, such as the central business district (CBD), still suffer from lasting exposure to vehicle emissions due to the heavy traffic and compact built environment. So far, these threats tend to be underestimated because of the lack of high-resolution spatial information of air pollution across the island, as suggested by Velasco and Roth (Velasco and Roth, 2012). Worse still, the health risk related to pollutant exposure may increase under hot and humid microclimates (Qian et al., 2008), which dominate the deep street canyons in Singapore.

Recently, Singapore government has drafted a new master plan (URA, 2019) which will guide the city's developments over the next 10 to 15 years. As outlined in this master plan, the CBD will be transformed into a vibrant mixed-use district. To this end, more public spaces, housings and amenities will be introduced into the developing marina bay district. With the concession of the overall building density, pedestrian spaces are expected to have a wider range of layouts and more linkages, especially at the ground level. This vision offers the city center an opportunity to optimize its outdoor ventilation by appropriately arranging and linking a variety of pedestrian spaces (Fig. 1).

The optimization of pedestrian-level flow and pollutant dispersion in high-density urban areas has been brought into focus in recent decades (Blocken, 2018; Tominaga and Stathopoulos, 2011). With the advances of wind tunnel and Computational Fluid Dynamics (CFD) techniques, the effects of design strategies of street canyons and buildings on improving outdoor ventilation and air quality have been evaluated parametrically by many studies. For street canyon designs, a large number of investigations have been conducted into flow and pollutant dispersion behaviors in uniform street canyons (Ali-Toudert and Mayer, 2006; Oke, 1988; Tsai and Chen, 2004) and orthogonal street intersections (Kim and Baik, 2004; Moonen et al., 2012; Soulhac et al., 2009) with various aspect ratios and orientations. More recently, a few research focuses have been given into non-uniform street canyons and non-orthogonal street intersections. For example, Ramponi et al. (Ramponi et al., 2015) explored the ventilation efficiency in parallel street canyons with unequal street widths and suggested the benefit of introducing a wider main street which acted as a sink of clean air. He et al. (He et al., 2019) evaluated the ventilation performance in four-way street intersections with various intersection angles and proposed orientation design strategies for the upwind and downwind streets respectively. Additionally, some studies have also been conducted inside actual street canyons and intersections (Aghamolaei et al., 2020; Borrego et al., 2016; Lee and Kwak, 2020; Murena et al., 2009; Shen et al., 2017; Thaker and Gokhale, 2016). For building designs, one of the main study focuses was on the effects of building permeability/density, such as building separations, setbacks, and voids/lift-ups, on improving air ventilation and quality (Sha et al., 2018; Wen et al., 2017; Yuan et al., 2014). Another main study focus was on the effects of non-uniform building geometries/dimensions, such as building height variability, on redirecting and mitigating in-canyon air pollutants (Chen et al., 2017; Gu et al., 2011; Hang et al., 2012a). Practical urban design guidelines, such as “Qualitative guidelines on air ventilation” (HKPD, 2015) of Hong Kong, have also been achieved as deliverables of the relevant research.

Despite much research on a number of design parameters of street canyons (e.g., aspect ratios and orientations) and buildings (e.g., permeability/density and height variability), the literature review reveals insufficient investigation into the patterns of linear open spaces. Particularly, compared with the uniform linear open spaces (e.g., vehicle roads), the linear open spaces with diverse morphologies (e.g., pedestrian spaces inside urban blocks) attracted much less attentions. Consequently, it is still unclear how a variety of pedestrian spaces inside urban blocks should be linked to form breezeways (Ng, 2009) and improve urban ventilation. The studies on the linked pedestrian spaces have presumably been neglected due to the presence, in many high-density urban areas, of a morphology

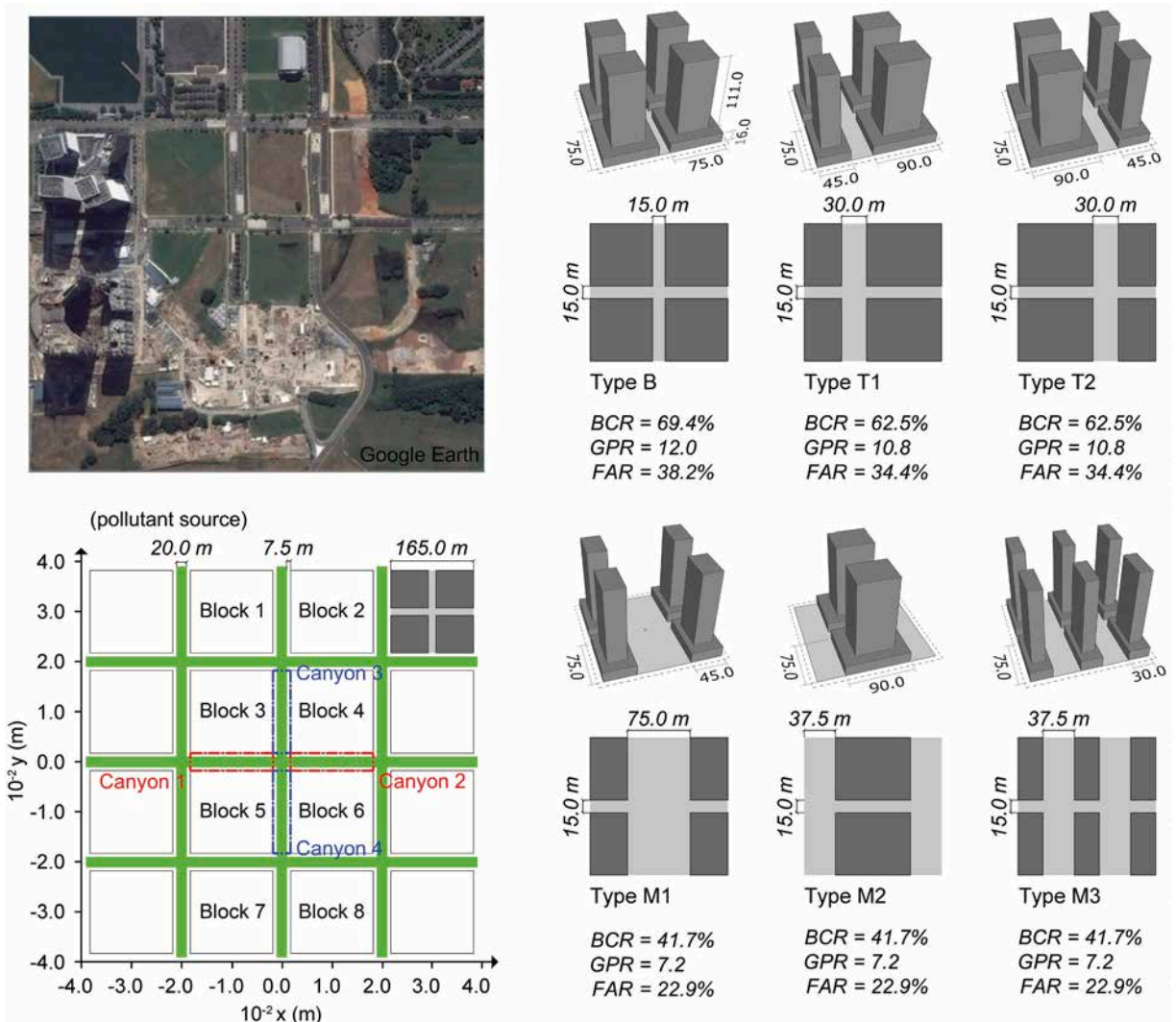


Fig. 2. A fixed road network abstracted from Singapore's developing CBD and six types of urban blocks in three levels of high-density: Baseline (B), Typical (T), and Moderate (M) (BCR: building coverage ratio; GPR: gross plot ratio; and FAR: frontal area ratio).

with little or total absence of pedestrian spaces inside urban blocks. This, however, is not necessarily the typical situation in Singapore's CBD and other high-density and mixed-use urban areas.

To fill the gaps, the purposes of this study are twofold. First, it attempts to cross-compare the effects of various linking patterns of pedestrian spaces on outdoor ventilation and air quality in high-density urban areas by numerical simulations. Second, based on the findings in the first objective, it attempts to provide relevant design recommendations for linking pedestrian spaces and improving air ventilation. As mentioned earlier in this section, the trend of vibrant mixed-use developments in high-density urban areas expects a substantial increase of pedestrian-level activities and risks of exposure to vehicle emissions. As such, a properly-linked and well-ventilated pedestrian spaces is essential to safeguard the public's health.

## 2. Methodology

### 2.1. Urban model developments

In this section, various generic urban models to be evaluated by CFD simulations were developed. There are two steps: 1) to abstract a road network and six types of basic urban blocks based on actual high-density urban morphologies (Section 2.1.1); and 2) to develop sixteen scenarios of urban models by using various combinations of the six types of basic urban blocks along with the road network (Section 2.1.2).

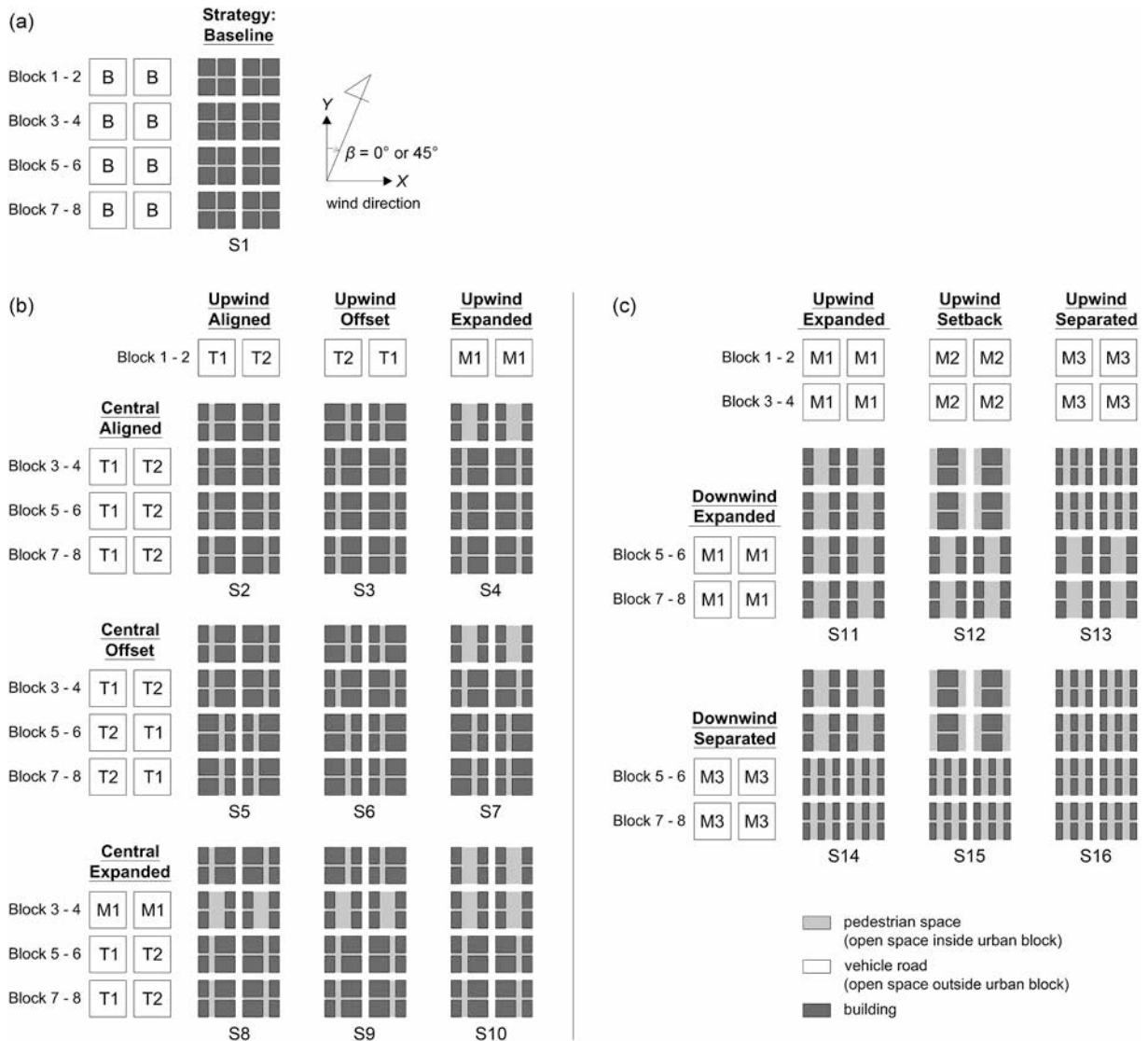


Fig. 3. Urban models developed by various linking patterns, i.e., (a) the baseline; (b) combinations of aligned, offset and expanded patterns; and (c) combinations of expanded, setback and separated patterns, of six types of urban blocks (Fig. 2).

2.1.1. Road network and urban blocks

At the first step, an orthogonal road network was abstracted from a developing high-density and mixed-use area (Fig. 2) at Singapore's CBD. This road network forms a uniform grid plan for all urban blocks. Together with the road network, six types of basic urban blocks were abstracted to represent three levels of typical high-density at the CBD, i.e., Baseline (B), Typical (T), and Moderate (M) high-density.

The B level refers to the typical maximum allowable density in high-density urban blocks in the new master plan (URA, 2021). At this level, the baseline urban block type (i.e., Type B) was abstracted from the conventional commercial block design (i.e., narrow pedestrian spaces with bulky podiums). The T and M levels refer to the density with concession to allow more pedestrian spaces in mixed-use urban blocks (URA, 2021). At these two levels, five urban block types, transformed from Type B, were used to represent different basic patterns of pedestrian spaces (i.e., T1/T2: offset pattern, M1: expanded pattern, M2: setback pattern, and M3: separated pattern). The three levels of high-density range from Building Coverage Ratio (BCR) (i.e., footprint area of buildings divided by land area of the block) of 70% to 40%, Gross Plot Ratio (GPR) (i.e., gross floor area of buildings divided by land area of the block) of 12 to 7, and Frontal Area Ratio (FAR) (i.e., building frontal area perpendicular to the axis of main pedestrian spaces divided by land area of the block) of 40% to 20%.

2.1.2. Urban models with various linking patterns of pedestrian spaces

At the second step, sixteen scenarios of urban models were developed by combining the six types of basic urban blocks (Fig. 2),

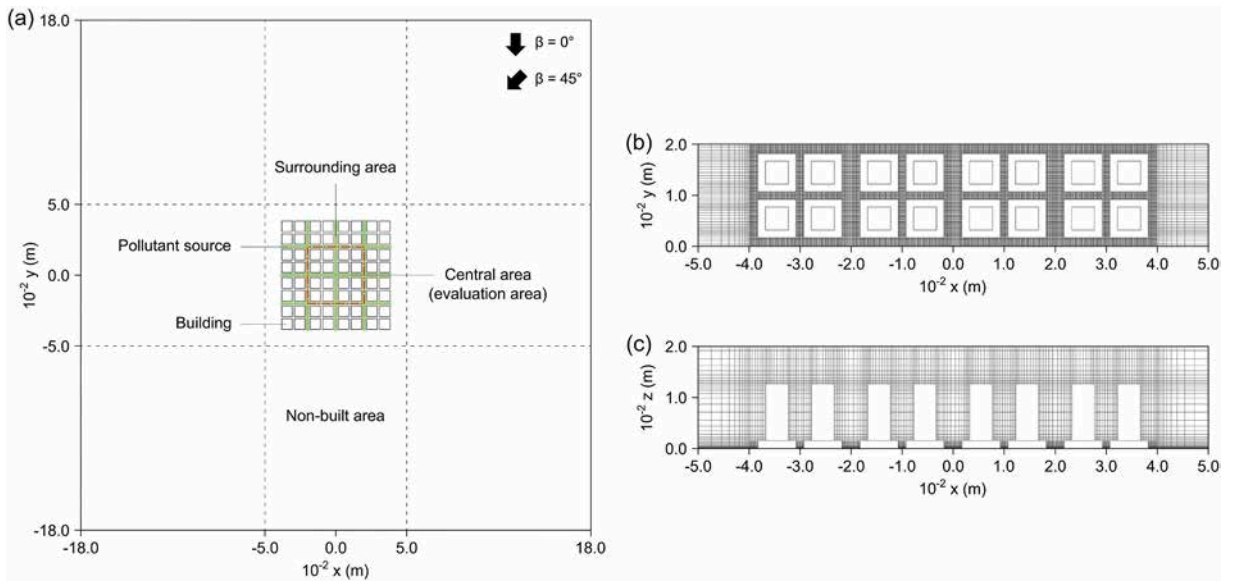


**Fig. 4.** Computational domain and mesh arrangements near buildings: (a) domain in horizontal dimension; (b) mesh in horizontal dimension; and (c) mesh in vertical dimension.

abstracted in Section 2.1, in the grid plan. As shown in Fig. 3, the baseline scenario (S1) represents the conventional high-density urban morphology, consisting of Type B urban blocks with the highest density. The other scenarios (S2 – S16) consider concession in density by transforming the urban blocks from Type B to others. Among these scenarios, S2 – S10 combine Types T1, T2 and M1 at the upwind (i.e., blocks 1 and 2) and center (i.e., blocks 3–6), linking the pedestrian spaces with aligned, offset, and expanded patterns. S11 – S16 combine Types M1, M2 and M3 at the upwind (i.e., blocks 1–4) and downwind (i.e., blocks 5–8), linking the pedestrian spaces with expanded, setback and separated patterns.

## 2.2. CFD simulations

In this section, CFD simulations were conducted to the sixteen scenarios of urban models developed in Section 2.1. CFD technique has been increasingly used as an alternative to wind tunnel technique for evaluating urban flow and pollutant dispersion with the advances in computer powers (Blocken, 2018; Tominaga and Stathopoulos, 2013). In this study, the simulation works were conducted by a commercial CFD code, scSTREAM (version 14). The steady-state Reynolds-averaged Navier-Stokes (RANS) model was applied to solve both turbulent flow and pollutant dispersion in isothermal conditions. A number of studies (Tominaga and Stathopoulos, 2011; Antoniou et al., 2017; Mazarakis et al., 2016; Salim et al., 2011) have compared the pros and cons between two prevailing CFD turbulent models, RANS and Large-eddy Simulation (LES). Compared with LES, RANS is not able to reproduce the instantaneous motions of large eddies due to the parameterization in calculation. However, RANS is used more frequently than LES so far due to its better balance between efficiency (i.e., much less computational cost) and accuracy (i.e., comparable simulation results on a time-averaged basis). Given the large number of scenarios to be simulated and the limited computer power, RANS is considered a “fit-for-purpose” turbulent model for this study.

### 2.2.1. Turbulent flow model

The flow-related computational settings of the current CFD code follow the guidelines (Tominaga et al., 2008) published by Architectural Institute of Japan (AIJ) and have been validated by a wind tunnel experiment conducted at Department of Building, National University of Singapore (He et al., 2019). Among these settings, the size of the computational domain was prescribed to  $3600 \times 3600 \times 550 \text{ m}^3$  ( $X \times Y \times Z$ ), as shown in Fig. 4a, to allow sufficient buffer distances between the urban model and domain boundaries. Cartesian grids were used inside the domain, where finer cells cover the podium structures and pedestrian spaces with the maximum stretching ratio of 1.3, as shown in Fig. 4b and c. The total cell number generated in each simulation scenario is around 6 million.

At the domain inlet, the vertical inflow profiles of wind velocity ( $U$ ), turbulence kinetic energy ( $k$ ) and turbulence dissipation rate ( $\epsilon$ ) were calculated by the following Eqs. (Tominaga et al., 2008):

$$U = \frac{U_*}{\kappa} \ln \left( \frac{z + z_0}{z_0} \right) \quad (1)$$

**Table 1**  
Traffic counts per hour ( $N_i$ ) (Velasco and Tan, 2016) and emission factors ( $K_i$ ) (Ng and Chau, 2014) of vehicle type  $i$ .

Vehicle type $i$	$N_i$ (-)	$K_i$ (g h <sup>-1</sup> )
Passenger cars	1406	3.62
Taxis	549	3.37
Motorcycles	177	24.2
Buses	166	4.69
Light good vehicles	197	1.04
Heavy good vehicles	25	2.39

$$k = \frac{U_*^2}{\sqrt{C_\mu}} \quad (2)$$

$$\varepsilon = \frac{U_*^3}{\kappa(z + z_0)} \quad (3)$$

where the friction velocity ( $U_*$ ) was estimated by Singapore's long-term average wind speed (i.e., 2.65 m/s at 15 m) at Changi climate station (MSS, 2011); the roughness length ( $z_0$ ) was set to 1 m, representing Singapore's urban terrain characteristics; the von Karman constant ( $\kappa$ ) was set to 0.4; and the model constant ( $C_\mu$ ) was set to 0.09. Correspondingly, the outflow was set to be natural.

The domain ground applied  $z_0$  of 0.4 m and 0.03 m in the non-built area (i.e., central area) and built-up area (i.e., surrounding area) respectively. This setting minimized the inflow inhomogeneity (Blocken et al., 2007) and meanwhile ensured the high resolution of computational grids near the ground (He et al., 2018). The domain top and lateral walls applied free slip conditions. In the domain, the RANS standard  $\kappa$ - $\varepsilon$  model was selected to solve the turbulent flow as determined by the validation study (He et al., 2019).

### 2.2.2. Pollutant dispersion model

The pollutant transport model of the current CFD code was based on the governing equation of time-averaged pollutant concentration:

$$\frac{\partial U_j c}{\partial x_j} = \frac{\partial}{\partial x_j} \left[ (D_m + D_t) \frac{\partial c}{\partial x_j} \right] + S \quad (4)$$

$$D_t = \frac{\nu_t}{Sc_t} \quad (5)$$

where  $x_j$  and  $U_j$  are the coordinates and velocity component in direction  $j$ , respectively;  $c$  is the time-averaged concentration (kgm<sup>-3</sup>);  $D_m$  and  $D_t$  are the molecular and turbulent diffusivity of a diffusive species (m<sup>2</sup>s<sup>-1</sup>), respectively;  $S$  is the source terms;  $\nu_t$  is the kinematic eddy viscosity; and  $Sc_t$  is the turbulent Schmidt number, where 0.9 is employed in the current CFD code (Cradle, 2018).

To reproduce the pollutants from vehicles, the simulations set all road surfaces in the urban models (i.e., green areas in Fig. 2) as uniformly-distributed sources of emissions. Carbon monoxide (CO), as one of the harmful air pollutants reviewed in Section 1, was selected as the tracer gas. Based on the traffic counts of six vehicle types at Singapore's CBD and the corresponding vehicle emission factors (Table 1), the input CO mass flow rate ( $M$ ) per unit road length was calculated to be 0.000037825 kgm<sup>-1</sup> s<sup>-1</sup> using the following equation:

$$M = \frac{\sum_{i=1}^n N_i K_i}{L} \quad (6)$$

where the traffic flow of vehicle type  $i$  ( $N_i$ ) was counted by Velasco and Tan (Velasco and Tan, 2016) at a five-lane segment of Raffles Quay bordered by Cross and Telegraph streets during the morning peak hours; the emission factor of vehicle type  $i$  ( $K_i$ ) was provided by Ng and Chau (Ng and Chau, 2014); and the length of the target street segment ( $L$ ) is 90 m.

To ensure the accuracy of the pollutant transport model, a validation was conducted by using the wind tunnel data in a pollutant dispersion experiment from Tominaga and Stathopoulos (Tominaga and Stathopoulos, 2011). This set of experimental data has been widely used to validate pollutant behaviors in CFD for sharp-edged building arrays (Tominaga and Stathopoulos, 2011; Yuan et al., 2014; Mei et al., 2019), hence fitting the morphology of urban models used in the current study. The CFD validation settings and results are attached in the Appendix of this paper.

## 3. Results and discussion

### 3.1. Indicators of outdoor wind condition and air quality

This study used two indicators, normalized wind velocity ( $U^*$ ) and pollutant concentration ( $c^*$ ) (Hang et al., 2012b), to evaluate wind conditions and air quality in various scenarios of linking patterns of pedestrian spaces:

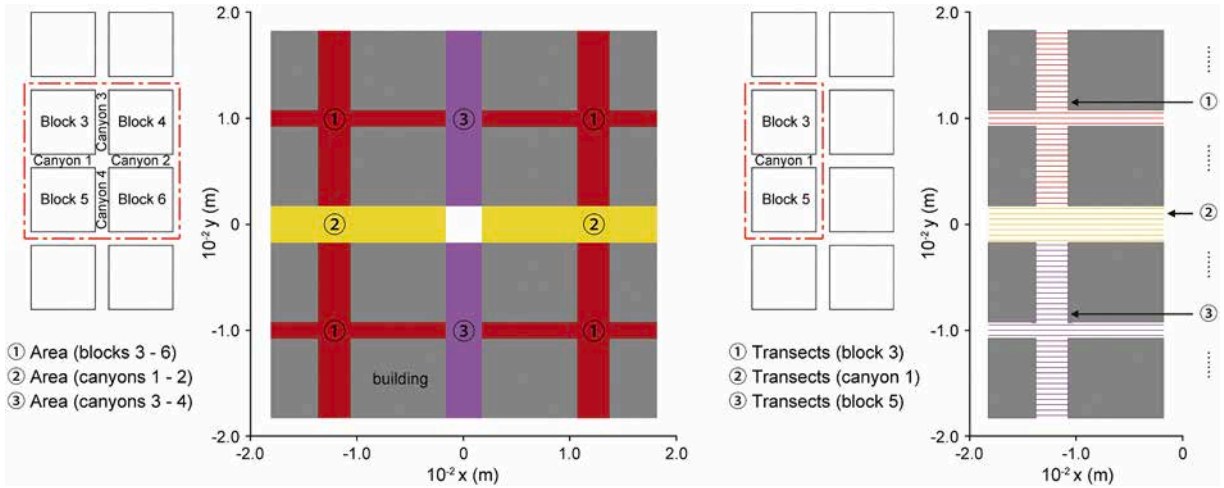


Fig. 5. Diagram of areas and transects at open spaces inside urban blocks and vehicle roads for averaging  $U^*$  and  $c^*$  at the height for evaluation.

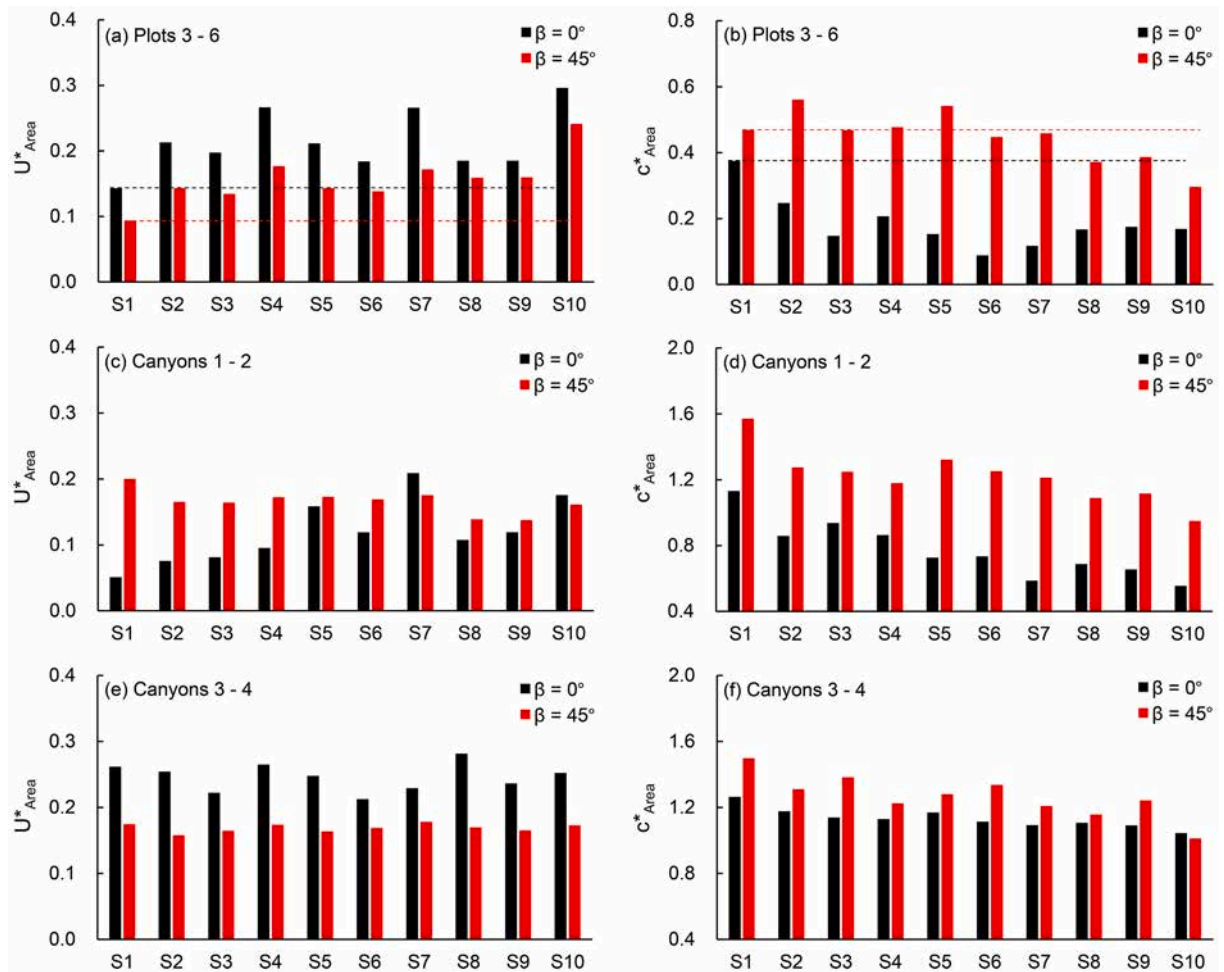


Fig. 6. Normalized area-averaged velocity ( $U^*_{Area}$ ) and concentration ( $c^*_{Area}$ ) at pedestrian level in S1 – S10 (baseline: S1; central aligned: S2 – S4; central offset: S5 – S7; central expanded: S8 – S10; upwind aligned: S2, S5, S8; upwind offset: S3, S6, S9; upwind expanded: S4, S7, S10).

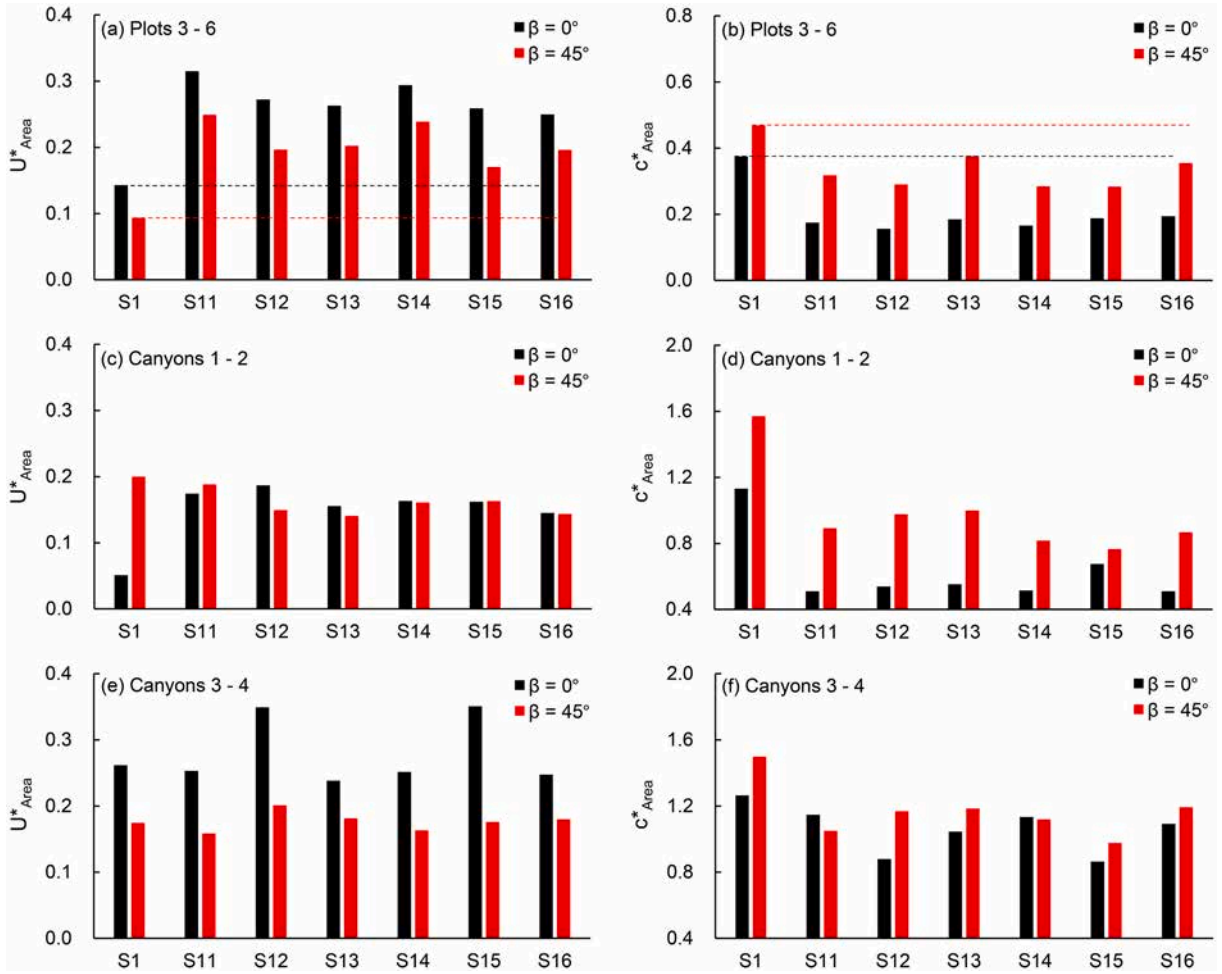


Fig. 7. Normalized area-averaged velocity ( $U^*_{Area}$ ) and concentration ( $c^*_{Area}$ ) at pedestrian level in S11 – S16 (baseline: S1; downwind expanded: S11 – S13; downwind separated: S14 – S16; upwind expanded: S11, S14; upwind setback: S12, S15; upwind separated: S13, S16).

$$U^* = \frac{U}{U_\infty} \tag{7}$$

$$c^* = \frac{cU_\infty WH}{ML} \tag{8}$$

where  $U_\infty$  refers to the free-stream wind velocity ( $\text{ms}^{-1}$ );  $W$  refers to the road width (20 m); and  $H$  refers to the pedestrian-level height (2 m). The defined  $U^*$  and  $c^*$  indicate the ratios of the simulated  $U$  and  $c$  to the reference  $U$  and  $c$  in free-stream conditions.

To evaluate the overall performance of  $U^*$  and  $c^*$ , they were calculated on area-averaged basis at the height for evaluation. Specifically, the area-averaged  $U^*$  and  $c^*$  were calculated at three categories of open spaces of the central area, i.e., open spaces at blocks 3–6, canyons 1–2, and canyons 3–4 (Fig. 5), using the following equations:

$$U^*_{Area} = \frac{\sum_{x=i,y=j}^n U^*_{xy}}{n} \tag{9}$$

$$c^*_{Area} = \frac{\sum_{x=i,y=j}^n c^*_{xy}}{n} \tag{10}$$

where  $x$  and  $y$  are the coordinates of data points at a calculation area ( $x$  and  $y$  with intervals of 5 m);  $U^*_{xy}$  and  $c^*_{xy}$  are  $U^*$  and  $c^*$  at these data points respectively; and  $n$  is the number of these data points.

To further evaluate the fluctuating performance of pollutant dispersion along the axis of the main pedestrian spaces,  $c^*$  was calculated on transect-averaged basis at the height for evaluation. Specifically, the transect-averaged  $c^*$  was calculated at equidistant transects ( $c^*_{Transect}$ ) covering the pedestrian spaces at block 3, canyon 1, and block 5 (Fig. 5), using the following equation:

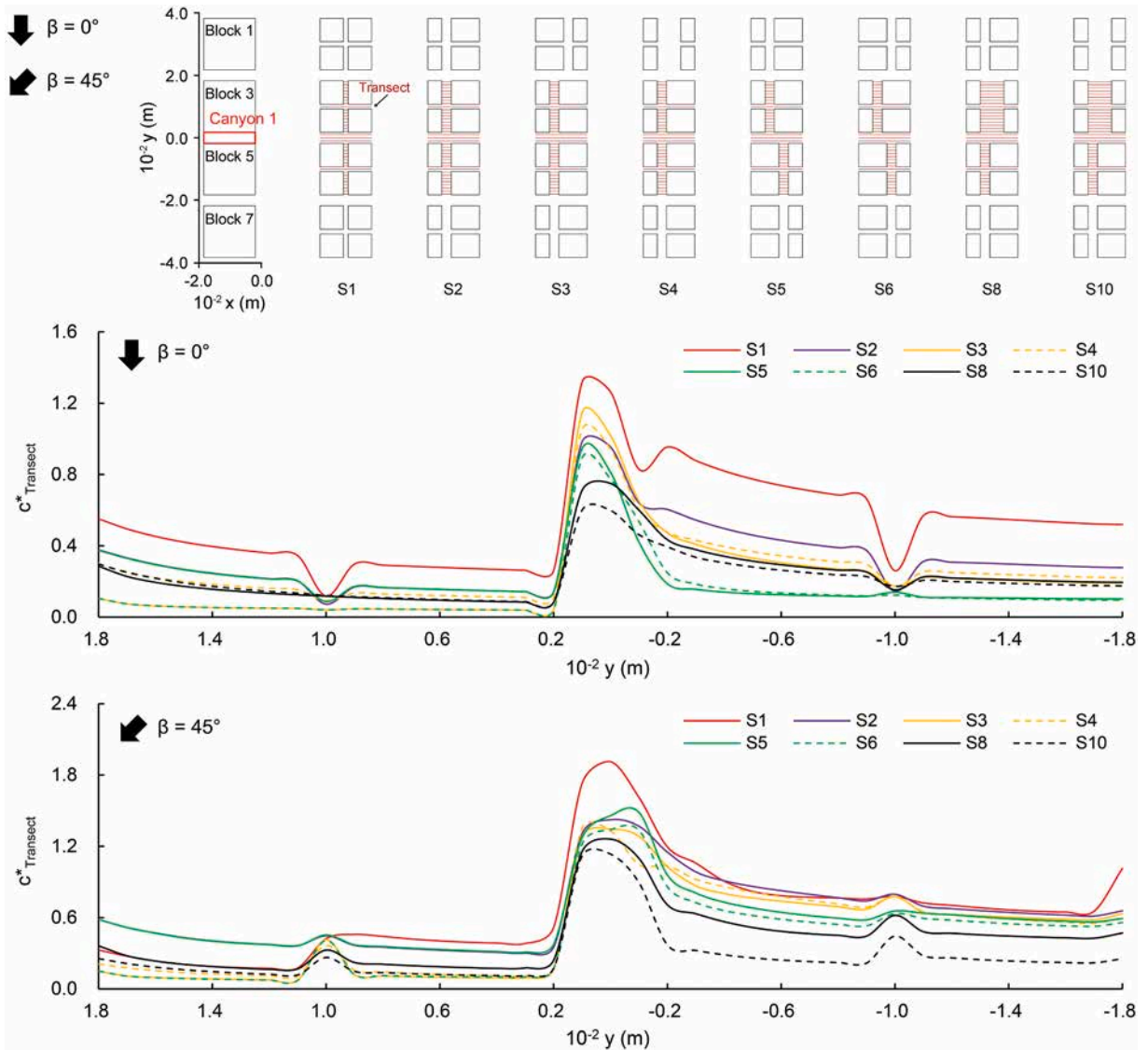


Fig. 8. Normalized transect-averaged concentration ( $c^*_{Transect}$ ) at pedestrian level in S1 – S10.

$$c^*_{Transect} = \frac{\sum_{x=1}^m c^*_x}{m} \tag{11}$$

where  $x$  is the coordinates of data points at each calculation transect ( $x$  ranging from  $-180$  to  $-20$  m with intervals of  $5$  m);  $c^*_x$  is  $c^*$  at these data points; and  $m$  is the number of these data points.

### 3.2. Overall performance: Area-based analysis results

#### 3.2.1. Cross-comparison of aligned, offset and expanded pedestrian spaces

To understand the overall performance in different scenarios of urban models (S1 – S10), the pedestrian-level wind velocity and pollutant concentration at both urban blocks and road canyons are analyzed on area-averaged basis in two prevailing wind directions. As shown in Fig. 6, all scenarios have worse air quality in the oblique wind direction ( $\beta = 45^\circ$ ), since pollutants from upwind vehicle roads in both  $x$  and  $y$  directions can be directed into the center of the urban area.

At the urban blocks (Fig. 6a–b), which are the main focus of this study, reducing building density from the baseline (S1 ( $BCR = 70\%$ )) to other scenarios (S2 – S10 ( $BCR > 50\%–60\%$ )) significantly increases  $U^*_{Area}$  regardless of wind directions. With the enhanced prevailing wind, substantial decreases of  $c^*_{Area}$  are observed when  $\beta = 0^\circ$ . However, the enhanced prevailing wind cannot guarantee a lower  $c^*_{Area}$  when  $\beta = 45^\circ$ . There are two main reasons. First, the enhanced oblique flow on one hand dilutes pollutants in the stream-

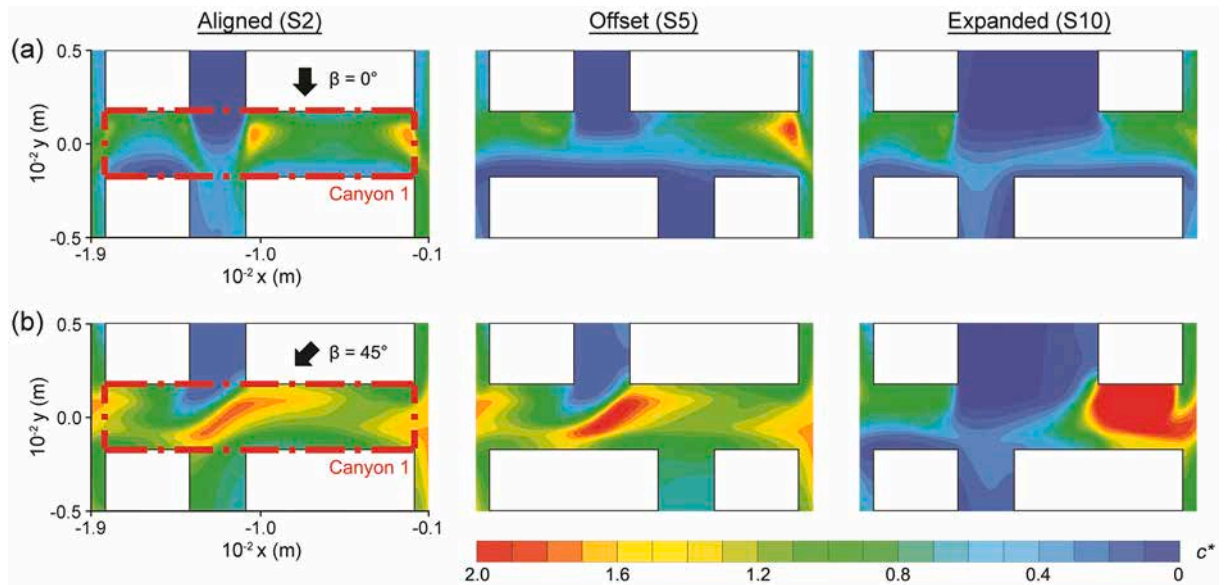


Fig. 9. Normalized pollutant concentration ( $c^*$ ) at pedestrian level of canyon 1 with aligned, offset, and expanded patterns.

wise direction (i.e.,  $y$  direction), and on the other hand introduces more pollutants in the span-wise direction (i.e.,  $x$  direction). Second, the enhanced oblique flow is tendentially more complex due to its stronger vorticity (Kim and Baik, 2004) and may complicate the pollutant dispersion behaviors. Compared with the upwind aligned patterns (S2, S5 and S8), the upwind expanded patterns (S4, S7 and S10) enhance both the wind conditions and pollutant dispersion; and the upwind offset patterns (S3, S6 and S9) enhance the pollutant dispersion rather than wind velocity, suggesting that the enhanced pollutant dispersion is driven by the changes of flow directions. Similar results are also observed in the comparison among the central aligned (S2 – S4), central expanded (S8 – S10), and central offset (S5 – S7) patterns.

At the road canyons, although the ambient air quality is less critical to the outdoor activities than that at the urban blocks, adequate ventilation is still required to reduce the pollutant concentration near the source. At canyons 1–2 (Fig. 6c–d), similar as at the urban blocks, the expanded and offset patterns are generally more effective in improving the air ventilation and quality than the aligned patterns. However, the wind conditions and air quality at canyons 3–4 (Fig. 6e–f) are less sensitive to the linking patterns of pedestrian spaces.

### 3.2.2. Cross-comparison of expanded, setback and separated pedestrian spaces

For S11 – S16, the cross-comparison of  $U^*_{Area}$  and  $c^*_{Area}$  at both urban blocks and road canyons is shown in Fig. 7. At the urban blocks (Fig. 7a–b), compared with S2 – S10 ( $BCR > 50\%–60\%$ ), the lower density in S11 – S16 ( $BCR > 40\%$ ) further enhances the flow. Significant improvements on the air quality are also observed when  $\beta = 45^\circ$  due to the higher permeability in the stream-wise direction (i.e.,  $y$  direction). The linking patterns of the pedestrian spaces in S11 – S16 still affect both  $U^*_{Area}$  and  $c^*_{Area}$ , although their effects are less significant than those in S2 – S10. In general, the upwind expanded patterns (S11 and S14) have the highest  $U^*_{Area}$  and lowest  $c^*_{Area}$ , while the upwind separated patterns (S13 and S16) generate the weakest wind conditions and poorest air quality.

At canyons 1–2 (Fig. 7c–d), the effects of the linking patterns on  $U^*_{Area}$  and  $c^*_{Area}$  are relatively small, and slightly better air ventilation and quality is observed in the upwind expanded patterns (S11 and S14). At canyons 3–4 (Fig. 7e–f), much larger  $U^*_{Area}$  and smaller  $c^*_{Area}$  are observed in the upwind setback patterns (S12 and S15) when  $\beta = 0^\circ$ . In these two patterns, the pedestrian spaces are adjacent to the vehicle roads to form wider air paths, which help to generate stronger stream-wise flow and accelerate the pollutant dispersion.

### 3.3. Fluctuating performance: Transect-based analysis results

#### 3.3.1. Cross-comparison of aligned, offset and expanded pedestrian spaces

To understand the pollutant dispersion along the axis of the main pedestrian spaces of different linking patterns (S1 – S10), the distribution of pollutant concentration at block 3, canyon 1, and block 5 are analyzed on transect-averaged basis. As described in Fig. 8,  $c^*_{Transect}$  peaks at canyon 1, where the pollutant source is located, while higher  $c^*_{Transect}$  is observed at block 5 than block 3 due to the combined effects of weaker wind conditions and heavier pollutant accumulation at the downwind.

Among different linking patterns, the offset and expanded patterns are generally more effective to mitigate the pollutants than the aligned patterns. When  $\beta = 0^\circ$ , for example, the maximum  $c^*_{Transect}$  at canyon 1 and block 5 in the central expanded patterns (S8 and S10) and central offset patterns (S5 and S6) is half of those in the central aligned patterns (S2 – S4). Furthermore, compared with the expanded patterns, the offset patterns can be more effective to improve the air quality although they have higher building density. In

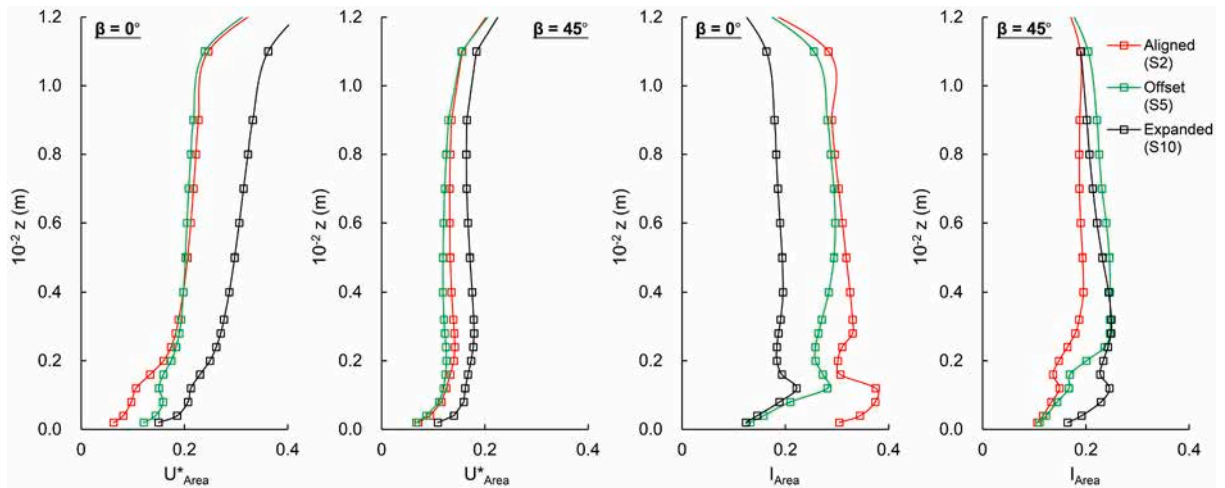


**Fig. 10.** Normalized area-averaged velocity ( $U^*_{Area}$ ) and area-averaged turbulence intensity ( $I_{Area}$ ) at different heights of canyon 1 with aligned, offset, and expanded patterns.

particular, the lowest  $c^*_{Transect}$  is observed when the pedestrian spaces are offset at both the upwind and central blocks (S6) instead of only offsetting either the upwind (S3) or central (S5) pedestrian spaces. The better air quality in the offset patterns is mainly attributed to the larger drag force formed by the building windward facades at the road canyons as suggested by some previous studies (e.g. (Ahmad Zaki et al., 2012; Li et al., 2015)). The larger drag force enhances the span-wise flow and vertical mixing, which therefore accelerate the pollutant dispersion.

When  $\beta = 45^\circ$ , the expanded patterns perform better than the offset patterns on improving air quality especially at the downwind, as they introduce stronger stream-wise (i.e.,  $y$  direction) flow which prevents the span-wise (i.e.,  $x$  direction) pollutant transport into the road canyon and urban block. The lowest  $c^*_{Transect}$  is observed when the expanded patterns are arranged at both the upwind and central blocks (S10). This result is in line with previous studies (Ng, 2009; Ng et al., 2011), which suggested that more open spaces allow the prevailing wind to penetrate deeper into urban areas and improve air ventilation. In particular, the expanded pattern at the central blocks (S8) achieves lower  $c^*_{Transect}$  than that at the upwind blocks (S4), suggesting that the pollutant dispersion is more sensitive to the immediate surroundings instead of the upwind settings.

To complement the lack of understanding of the three-dimensional pollutant dispersion mechanism occurring at different linking intersections, the pedestrian-level concentration contours at three patterns of pedestrian spaces, i.e., aligned (S2), offset (S5), and expanded (S10), are plotted in Fig. 9 and the vertical profiles of  $U^*_{Area}$  and area-averaged turbulence intensity ( $I_{Area}$ ) at canyon 1 is plotted in Fig. 10.

At the pedestrian level, when  $\beta = 0^\circ$ , where the main pollutant source is at canyon 1, serious trapping of pollutants is observed at the stagnant zones sheltered by podiums in the aligned pattern. This situation is improved in the offset and expanded patterns as pollutants are dispersed by the enhanced horizontal flow. When  $\beta = 45^\circ$ , the prevailing wind transports exterior pollutants from canyon 3 and leads to pollutant accumulation at canyon 1 in both the aligned and offset patterns. The pollutants at the center of canyon 1 are dispersed in the expanded pattern as the exterior pollutants are condensed at the entry of canyon 1 by the enhanced stream-wise (i.e.,  $y$  direction) flow.

At the upper levels, the largest  $U^*_{Area}$  remains in the expanded pattern from the pedestrian level till the building roof level, indicating the pattern's best potential to optimize outdoor air quality. Comparable  $U^*_{Area}$  is observed in the offset pattern near the pedestrian level when  $\beta = 0^\circ$ , but it increases slowly with heights and may cause more trapping of pollutants in the upper air. The results of  $I_{Area}$  reveal the largest variations within the podium layer (i.e., 0–16 m), implying that the flow and dispersion behaviors are the most complex near the podiums. Within this layer, the largest  $I_{Area}$  is seen in the aligned pattern when  $\beta = 0^\circ$ , confirming that pollutants in this pattern is mainly dispersed by turbulent diffusivity and hence easily trapped. The offset and expanded patterns can take better use of the prevailing wind and displacement (i.e., span-wise and vertical) flow to disperse pollutants, as confirmed by their smaller  $I_{Area}$ .

### 3.3.2. Cross-comparison of expanded, setback and separated pedestrian spaces

For S11 – S16, the distribution of  $c^*_{Transect}$  is cross-compared in Fig. 11. Among these scenarios, the combinations with wider air paths (i.e., expanded and setback patterns) at the upwind and narrower air paths (i.e., separated patterns) at the downwind achieve the optimal air quality. For example, when  $\beta = 45^\circ$ , S14, which combines the upwind expanded pattern with the downwind separated pattern, achieves significantly lower  $c^*_{Transect}$  at canyon 1 and block 5 than other scenarios. This upwind-to-downwind diverged pattern introduces more prevailing wind from the upwind, and meanwhile generates more displacement (i.e., span-wise and vertical) flow at the road canyon which restricts the pollutants entering the downwind pedestrian spaces. In comparison, the upwind-to-downwind converged pattern (S13), which combines the upwind separated and downwind expanded patterns, leads to the highest

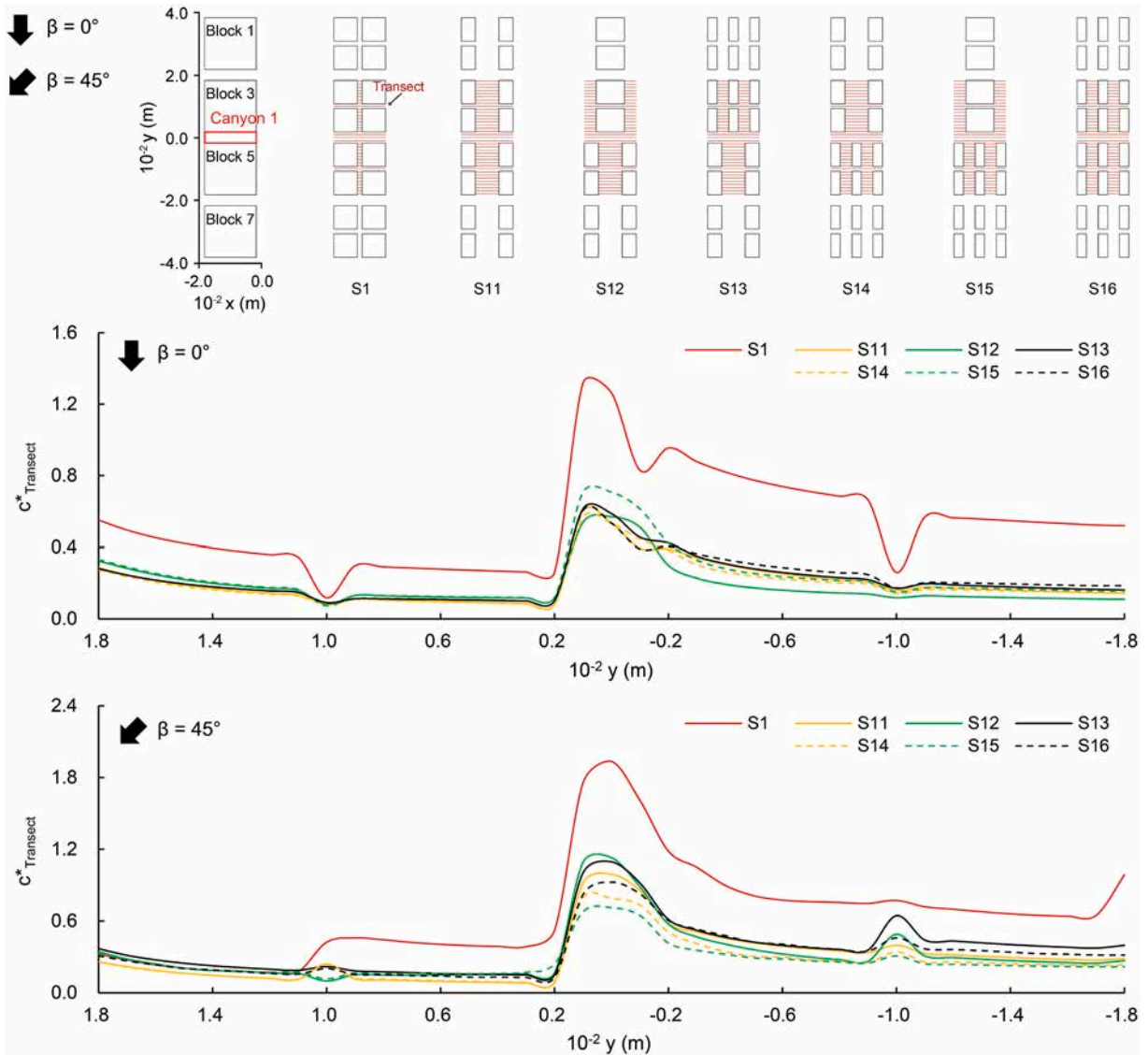


Fig. 11. Normalized transect-averaged concentration ( $c^*_{Transect}$ ) at pedestrian level in S11 – S16.

$c^*_{Transect}$ , which is double that in S14. The different results in S13 and S14 suggest pollutant dispersion can be improved by properly linking the pedestrian spaces even though building density is not compromised.

The pedestrian-level concentration contours at four linking patterns of pedestrian spaces, i.e., upwind expanded + downwind expanded (S11), upwind setback + downwind expanded (S12), upwind separated + downwind expanded (S13), and upwind expanded + downwind separated (S14), are shown in Fig. 12 and the vertical profiles of  $U^*_{Area}$  and area-averaged turbulence intensity ( $I_{Area}$ ) at canyon 1 is shown in Fig. 13.

At the pedestrian level, in the comparison among the three upwind patterns, the upwind setback and upwind separated patterns (S12 and S13) cause pollutant accumulation at the center of canyon 1 especially when  $\beta = 45^\circ$  due to the building wall effects (Yim et al., 2009). The accumulation occurs at the axis of main pedestrian spaces and can easily affect pedestrian activities. Different from the upwind setback and upwind separated patterns, the upwind expanded pattern (S11) disperses pollutants along the axis of main pedestrian spaces as it effectively channels the prevailing wind. In the comparison between the upwind-to-downwind converged (S13) and upwind-to-downwind diverged (S14) patterns, S13 generates a flow regime that easily transmits exterior pollutants from canyon 3 into canyon 1. In contrast, the flow regime in S14 enhances the horizontal pollutant dispersion in multiple directions and reduces exterior pollutants transmission from canyon 3.

At the upper levels, the  $U^*_{Area}$  profiles in the four patterns are similar when  $\beta = 0^\circ$ , while larger  $U^*_{Area}$  is observed in the two scenarios with upwind expanded patterns (S11 and S14) when  $\beta = 45^\circ$ . This result is consistent with those observed at the pedestrian level, suggesting that the upwind expanded pattern is effective to increase wind availability which is crucial to pollutant dispersion.

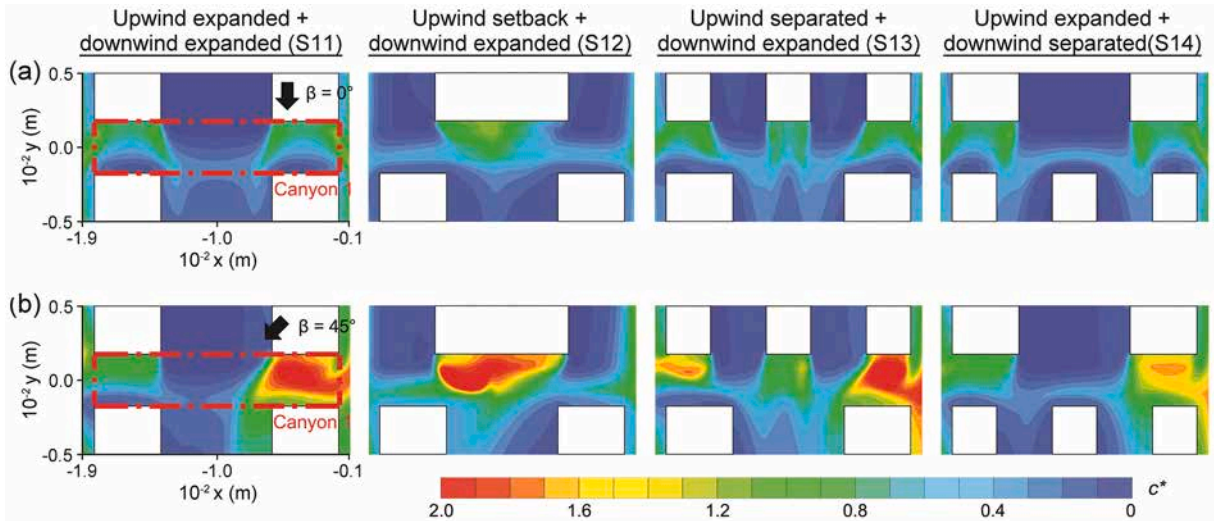


Fig. 12. Normalized pollutant concentration ( $c^*$ ) at pedestrian level of canyon 1 with expanded, setback, and separated patterns.

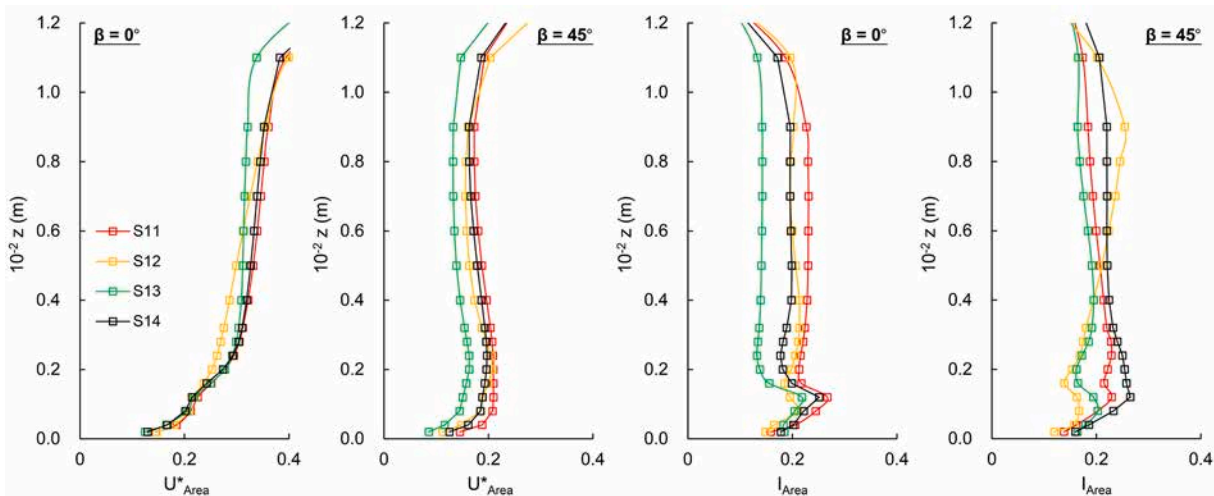


Fig. 13. Normalized area-averaged velocity ( $U^*_{Area}$ ) and area-averaged turbulence intensity ( $I_{Area}$ ) at different heights of canyon 1 in S11 – S14 with upwind/downwind expanded, setback, and separated patterns.

Additionally, it should be noted that, in most of the scenarios, the peak  $I_{Area}$  is observed at the roof level of podiums. At this level, relatively intensive turbulent diffusivity and vertical mixing may occur, hence increasing the chances of vertical air exchange to promote pollutant dilution.

Finally, to address the main effects (i.e., urban block permeability and morphological diversity) of the linking patterns of pedestrian spaces on outdoor wind conditions and air quality, all scenarios evaluated in Sections 3.2 and 3.3 are categorized into two sets based on the number of urban block type(s) at the central area (i.e., urban block type >1 (S5 – S10 and S12 – S15); urban block type = 1 (S1 – S4, S11 and S16)) for a correlation analysis.

As suggested in Fig. 14, both  $U^*_{Area}$  and  $c^*_{Area}$  show strong correlations with  $BCR$ , suggesting that increasing urban block permeability is a crucial consideration when linking the pedestrian spaces for improving air ventilation and pollutant dispersion. More importantly, the correlation result also suggests that, with the same  $BCR$ , the scenarios with multiple urban block types have similar  $U^*_{Area}$  but obviously lower  $c^*_{Area}$ , compared with the scenarios with a single urban block type. This result implies that increasing urban block morphological diversity is helpful to pollutant dispersion, and therefore should be taken into account when linking the pedestrian spaces.

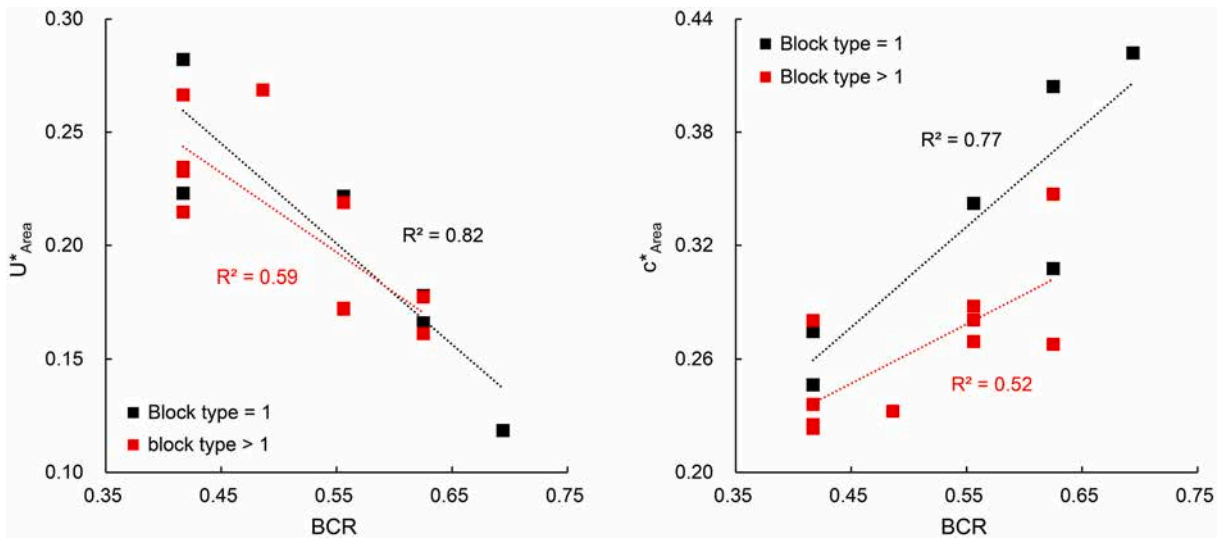


Fig. 14. Correlations of BCR with  $U^*_{Area}$  and  $c^*_{Area}$  in linking patterns consisting of single/multiple urban block types (note:  $U^*_{Area}$  and  $c^*_{Area}$  are the averaged values at plots 3–6 in two wind directions).

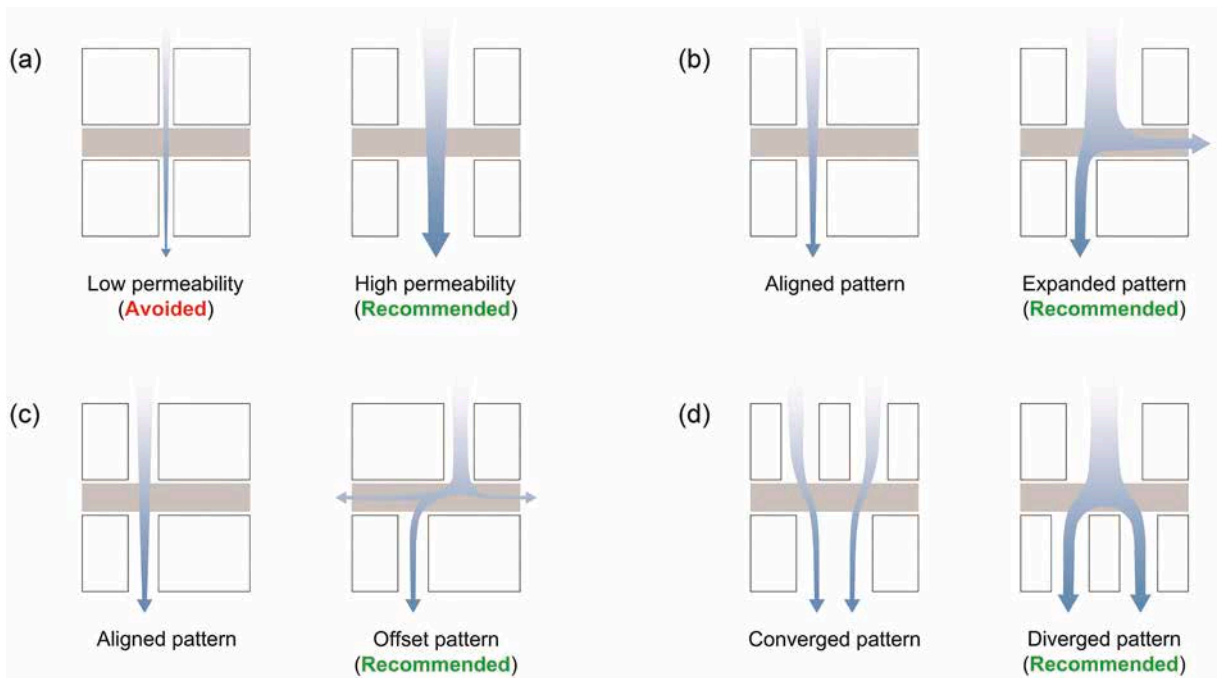


Fig. 15. Design recommendations of linking patterns of pedestrian spaces for optimizing wind and vehicular pollutant behaviors.

#### 4. Final discussion and conclusion

This study uses CFD simulations to investigate how pedestrian spaces should be linked to optimize the ambient flow and vehicular pollutant dispersion in tropical high-density urban areas. As such, a parametric study is conducted to evaluate various upwind-to-downwind linking patterns of pedestrian spaces in both typical ( $BCR > 60\%$ ) and moderate ( $BCR > 40\%$ ) high-density scenarios. Key findings and design recommendations for linking pedestrian spaces to improve air ventilation and quality in high-density urban areas are summarized in Fig. 15 and as follows:

- 1) *Pedestrian spaces and urban ventilation*: the linking patterns of pedestrian spaces are highly related to urban block permeability and morphological diversity, which affect air ventilation. In other words, air ventilation can potentially be optimized by adjusting the linking patterns of pedestrian spaces even without compromising building density.
- 2) *Pedestrian spaces and vehicle roads*: an explicit classification of pedestrian-level open spaces (i.e., pedestrian spaces and vehicle roads) is needed in an accurate urban ventilation assessment. Different types of open spaces may have very different flow and pollutant dispersion behaviors (Figs. 6 and 7), as well as different tolerances of pollutant exposures (EPA, 2021b; WHO, 2016). Particularly, more attention should be paid to the pedestrian spaces, since they are mainly responsible to outdoor activities and can adopt more flexible linking designs after the grid plan is established (He et al., 2018).
- 3) *Expanding pedestrian spaces*: in typical high-density urban areas ( $BCR > 60\%$ ), reducing building density can significantly improve both wind conditions and air quality in most scenarios. Ideally, the pedestrian spaces are recommended to be expanded from the upwind urban blocks (e.g., urban blocks at water front) till the target urban blocks, such as S10 in Fig. 8, in order to introduce more prevailing wind to enhance flow penetration and pollutant dispersion. Alternatively, it is also recommended to only expand the upwind pedestrian spaces adjacent to the target emission source (e.g., S8 in Fig. 8). This design recommendation suggests the needs to reduce building density and frontal blockages for improving urban ventilation, which is consistent with the existing urban design guidelines for high-density cities (Ng, 2009) as well as the discussions in previous studies (Yuan et al., 2014; Ng et al., 2011; Kubota et al., 2008).
- 4) *Offsetting pedestrian spaces*: in typical high-density urban areas, offsetting pedestrian spaces can be even more effective than expanding the pedestrian spaces in mitigating air pollutants, although it is less effective to increase wind velocity on average. Particularly, pedestrian spaces at both the upwind and the target urban blocks are recommended to be offset (e.g., S6 in Fig. 8), in order to increase drag force and generate more span-wise flow and vertical mixing. However, attentions should be paid to avoid a drastic increase of span-wise pollutant transmission when oblique prevailing wind occurs. This design recommendation provides the possibility to improve air quality without reducing building density, which is usually hard to be compromised in high-density urban developments (MND, 2000).
- 5) *Diverging pedestrian spaces*: in moderate high-density urban areas ( $BCR > 40\%$ ), urban blocks can have more design and combination options. When combining two urban blocks with different configurations, the one with wider air paths at the pedestrian level (e.g., expanded and setback patterns) should be arranged at the upwind in order to introduce more prevailing wind. Meanwhile, the one with narrower air paths (e.g., separated pattern) should be arranged at the downwind in order to generate more displacement (i.e., span-wise and vertical) flow to prevent transmitting the pollutants downwind. These upwind-to-downwind diverged patterns (e.g., S14 and S15 in Fig. 11) can considerably mitigate the pollutants at vehicle roads and downwind pedestrian spaces. In contrast, the upwind-to-downwind converged patterns (e.g., S13 in Fig. 11) are not recommended, since it can lead to relatively worse air quality.
- 6) *Diversifying urban block types*: overall, diversifying urban blocking types benefit air quality rather than wind conditions on average at pedestrian spaces in high-density urban blocks. With multiple urban block types, the pedestrian spaces are linked into variable patterns, which diverse the flow behaviors and optimize the pollutant dispersion. Furthermore, it also implies the needs to better understand the impacts of the more diverse linking patterns of pedestrian spaces, since they negatively affect the correlations of  $BCR$  with the performance of ambient wind conditions and air quality (Fig. 14).

Air ventilation at pedestrian spaces is crucial to both human health and comfort (Blocken et al., 2012; Höppe, 1999). The proposed urban design recommendations can be used for optimizing both outdoor wind conditions and air quality which are not always inversely related as proved in this study. They are particularly useful in high-density urban areas in tropical climates suffering from weak wind conditions, such as Singapore and Hong Kong. It is expected that a better ventilated pedestrian environment can encourage more outdoor activities, which potentially promote more sustainable and healthy living styles as well as more vibrant mixed-use urban developments.

## 5. Limitations and future works

This study focuses on the effects of linking patterns of pedestrian spaces, while the urban block models remain ideal and generic which exclude the effects of building design features (e.g., building permeability and variability) and street obstacles (e.g., trees). However, it should be noted that these features/obstacles might introduce significant perturbations to flow and pollutant behaviors in reality. Besides, this study mainly focuses on the flow and air pollutant behaviors at the pedestrian level, while some of their behaviors at the upper levels remain uncertain. Future work is necessary to investigate the flow and air pollutant exchanges at the roof and lateral boundaries of the urban canopy (Hang et al., 2012a) so as to better understand their mechanism in different urban patterns. Additionally, the current CFD technique (steady-state RANS) is known to have deficiency and unable to predict instantaneous flow and dispersion behaviors (Blocken, 2018). However, it provides reliable steady-state predictions on a spatially-averaged basis as revealed by the validations in the Appendix. Due to the lack of field measurement data, the current input pollutant mass flow rate in the simulations is estimated by traffic count data and may cause deviations on the absolute values in the output. However, this study enables comparisons of design options in terms of wind conditions and air quality, and identification of potential environmental problem at the pedestrian spaces for design improvements.

**Table 2**  
Boundary conditions of inflow and emission source in the wind tunnel experiment (Tominaga and Stathopoulos, 2011).

Inflow wind speed	Inflow turbulence intensity	Emission species	Emission concentration	Emission velocity
Interpolated profile	Interpolated profile	Ethylene (C <sub>2</sub> H <sub>4</sub> )	1000 ppm	0.456 m/s

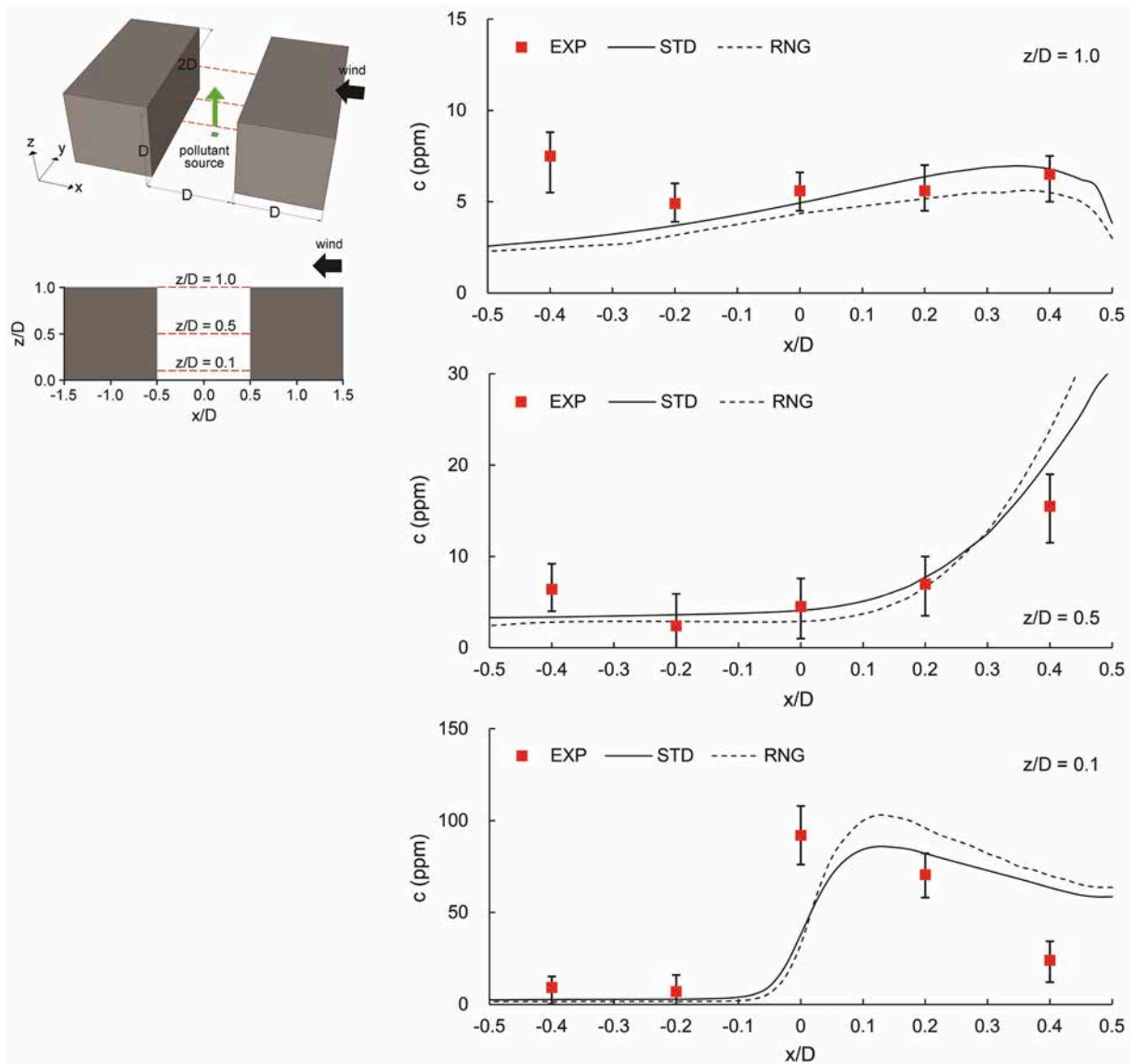


**Fig. 16.** Pollutant concentration ( $c$ ) results along the test lines at different heights: wind tunnel experimental data (EXP), and CFD simulation data with RANS standard  $\kappa\text{-}\epsilon$  (STD) and RNG  $\kappa\text{-}\epsilon$  (RNG) turbulence models.

**CRedit authorship contribution statement**

**Yueyang He:** Conceptualization, Methodology, Writing – original draft. **Abel Tablada:** Conceptualization, Methodology, Writing – review & editing, Supervision. **Ji-Yu Deng:** Conceptualization, Methodology, Writing – review & editing. **Yuan Shi:** Methodology, Writing – review & editing. **Nyuk Hien Wong:** Writing – review & editing, Supervision. **Edward Ng:** Writing – review & editing, Supervision, Funding acquisition.

## Declaration of Competing Interest

The authors declare that they have no known competing financial interests or personal relationships that could have appeared to influence the work reported in this paper.

## Acknowledgement

This research is supported by the General Research Fund (RGC Ref No. 14619121) from the Research Grants Council (RGC) of Hong Kong. It is partly supported by the Guangdong Basic and Applied Basic Research Foundation (No. 2022A1515010769). The authors highly appreciate the support of School of Design and Environment, National University of Singapore at the stage of CFD simulations and validation. The authors also highly appreciate reviewers for their insightful comments and suggestions on our research work.

## Appendix A. CFD validations

To validate the pollutant transport model of the current code for sharp-edged building arrays, CFD simulations were conducted to replicate the settings in a wind tunnel experiment (Tominaga and Stathopoulos, 2011). The settings include a street canyon model and boundary conditions of inflow and emission source as listed in Table 2. The effects of the materiality and roughness of the model facades in the experiment were excluded since they can be considered negligible and the relevant information is not availability. Both the RANS standard  $\kappa$ - $\epsilon$  (STD) and RNG  $\kappa$ - $\epsilon$  (RNG) turbulence models were tested in the simulations.

Fig. 16 depicts the street canyon model and the validation results of pollutant concentration at three heights. Overall, the numerical data (STD and RNG) is consistent with the experimental data (EXP) at all heights. The best agreement is seen at the middle height ( $z/D = 0.5$ ), while deviations are found at the upwind of the bottom height ( $z/D = 0.1$ ) and downwind of the top height ( $z/D = 1.0$ ). These deviations have also been found in validations with other CFD codes (Tominaga and Stathopoulos, 2011; Yuan et al., 2014; Mei et al., 2019). They can be caused by the deficiency of steady-state RANS which underestimates the turbulent diffusion due to the lack of data of reciprocating motions of large eddies. Consequently, steady-state RANS underestimates the span-wise pollutant transport driven by turbulent diffusivity and overestimates the stream-wise pollutant transport driven by in-canyon vortex along with prevailing wind. More accurate CFD results could be achieved by LES (Tominaga and Stathopoulos, 2011) or unsteady-state RANS (He et al., 2021b; 2022c), while much more computational cost is required.

Despite the deviations at limited test points, the overall fair agreement in the validation suggests the reliability of the current CFD model for predicting the in-canyon pollutant concentration on a spatially-averaged basis (i.e., line-averaged results at different heights) rather than a point basis. Thus, the current CFD model is appropriate for the evaluations based on area-averaged and transect-averaged data, and fits the purposes of the current study.

## References

- Aghamolaei, R., Azizi, M.M., Aminzadeh, B., Mirzaei, P.A., 2020. A tempo-spatial modelling framework to assess outdoor thermal comfort of complex urban neighbourhoods. *Urban Clim.* 33, 100665.
- Ahmad Zaki, S., Hagishima, A., Tanimoto, J., 2012. Experimental study of wind-induced ventilation in urban building of cube arrays with various layouts. *J. Wind Eng. Ind. Aerodyn.* 103, 31–40.
- Ali-Toudert, F., Mayer, H., 2006. Numerical study on the effects of aspect ratio and orientation of an urban street canyon on outdoor thermal comfort in hot and dry climate. *Build. Environ.* 41 (2), 94–108.
- Antoniou, N., Montazeri, H., Wigo, H., Neophytou, M.K.-A., Blocken, B., Sandberg, M., 2017. CFD and wind-tunnel analysis of outdoor ventilation in a real compact heterogeneous urban area: evaluation using “air delay”. *Build. Environ.* 126, 355–372.
- Blocken, B., 2018. LES over RANS in building simulation for outdoor and indoor applications: a foregone conclusion? *Build. Simul.* 11 (5), 821–870.
- Blocken, B., Stathopoulos, T., Carmeliet, J., 2007. CFD simulation of the atmospheric boundary layer: wall function problems. *Atmos. Environ.* 41 (2), 238–252.
- Blocken, B., Janssen, W., van Hooff, T., 2012. CFD simulation for pedestrian wind comfort and wind safety in urban areas: general decision framework and case study for the Eindhoven university campus. *Environ. Model. Softw.* 30, 15–34.
- Borrego, C., Amorim, J.H., Tchepel, O., Dias, D., Rafael, S., Sá, E., Pimentel, C., Fontes, T., Fernandes, P., Pereira, S., 2016. Urban scale air quality modelling using detailed traffic emissions estimates. *Atmos. Environ.* 131, 341–351.
- Buccolieri, R., Sandberg, M., Di Sabatino, S., 2010. City breathability and its link to pollutant concentration distribution within urban-like geometries. *Atmos. Environ.* 44 (15), 1894–1903.
- Chen, L., Hang, J., Sandberg, M., Claesson, L., Di Sabatino, S., Wigo, H., 2017. The impacts of building height variations and building packing densities on flow adjustment and city breathability in idealized urban models. *Build. Environ.* 118, 344–361.
- Cradle, 2018. scSTREAM version 14 user's guide basics of CFD analysis.
- EPA, 2021a. Research on health effects, exposure, & risk from mobile source pollution [cited 2021 March]; Available from: <https://www.epa.gov/mobile-source-pollution/research-health-effects-exposure-risk-mobile-source-pollution>.
- EPA, 2021b. Criteria air pollutants [cited 2021 March]; Available from: <https://www.epa.gov/criteria-air-pollutants>.
- Franco, V., Kousoulidou, M., Muntean, M., Ntziachristos, L., Hausberger, S., Dilara, P., 2013. Road vehicle emission factors development: a review. *Atmos. Environ.* 70, 84–97.
- Gu, Z.-L., Zhang, Y.-W., Cheng, Y., Lee, S.-C., 2011. Effect of uneven building layout on air flow and pollutant dispersion in non-uniform street canyons. *Build. Environ.* 46 (12), 2657–2665.
- Hang, J., Sandberg, M., Li, Y., 2009. Age of air and air exchange efficiency in idealized city models. *Build. Environ.* 44 (8), 1714–1723.
- Hang, J., Li, Y., Sandberg, M., Buccolieri, R., Di Sabatino, S., 2012a. The influence of building height variability on pollutant dispersion and pedestrian ventilation in idealized high-rise urban areas. *Build. Environ.* 56, 346–360.
- Hang, J., Li, Y., Buccolieri, R., Sandberg, M., Di Sabatino, S., 2012b. On the contribution of mean flow and turbulence to city breathability: the case of long streets with tall buildings. *Sci. Total Environ.* 416, 362–373.

- He, Y., Ren, C., Mak, H.W.L., Lin, C., Wang, Z., Fung, J.C.H., Li, Y., Lau, A.K.H., Ng, E., 2021a. Investigations of high-density urban boundary layer under summer prevailing wind conditions with Doppler LiDAR: a case study in Hong Kong. *Urban Clim.* 38, 100884.
- He, Y., Tablada, A., Wong, N.H., 2018. Effects of non-uniform and orthogonal breezeway networks on pedestrian ventilation in Singapore's high-density urban environments. *Urban Clim.* 24, 460–484.
- He, Y., Tablada, A., Wong, N.H., 2019. A parametric study of angular road patterns on pedestrian ventilation in high-density urban areas. *Build. Environ.* 151, 251–267.
- He, Y., Hii, D.J.C., Wong, N.H., Peck, T.G., 2021b. Unsteady RANS simulations of laboratory ventilation with chemical spills and gas leakages-Toward balanced safety and energy effectiveness. *Build. Environ.* 191, 107576.
- He, Y., Hii, D.J.C., Wong, N.H., Peck, T.G., 2022c. Sustainable laboratory evaluations: Optimized fume-hood-intensive ventilation and energy efficiency without compromising occupational safety and comfort. *J. Clean. Prod.* 130147.
- He, Yueyang, Yuan, Chao, Ren, Chao, Ng, Edward, 2022b. Urban ventilation assessment with improved vertical wind profile in high-density cities – comparisons between LiDAR and conventional methods. *J. Wind Eng. Ind. Aerodyn.*
- He, Y., Yuan, C., Ren, C., Wang, W., Shi, Y., Ng, E., 2022a. Urban ventilation assessment with improved vertical wind profile in high-density cities – investigations in nighttime extreme heat. *Build. Environ.* 109018 <https://doi.org/10.1016/j.buildenv.2022.109018>.
- HKPD, 2015. Qualitative guidelines on air ventilation, chapter 11 urban design guidelines, Hong Kong planning standards and guidelines. Hong Kong Planning Department (HKPD), Hong Kong.
- Höppe, P., 1999. The physiological equivalent temperature—a universal index for the biometeorological assessment of the thermal environment. *Int. J. Biometeorol.* 43 (2), 71–75.
- Kampa, M., Castanas, E., 2008. Human health effects of air pollution. *Environ. Pollut.* 151 (2), 362–367.
- Kim, J.-J., Baik, J.-J., 2004. A numerical study of the effects of ambient wind direction on flow and dispersion in urban street canyons using the RNG k-ε turbulence model. *Atmos. Environ.* 38 (19), 3039–3048.
- Krzyzanowski, M., Kuna-Dibbert, B., Schneider, J., 2005. Health effects of transport-related air pollution. WHO Regional Office Europe.
- Kubota, T., Miura, M., Tominaga, Y., Mochida, A., 2008. Wind tunnel tests on the relationship between building density and pedestrian-level wind velocity: development of guidelines for realizing acceptable wind environment in residential neighborhoods. *Build. Environ.* 43 (10), 1699–1708.
- Lee, S.-H., Kwak, K.-H., 2020. Assessing 3-D spatial extent of near-road air pollution around a signalized intersection using drone monitoring and WRF-CFD modeling. *Int. J. Environ. Res. Public Health* 17 (18), 6915.
- Li, B., Liu, J., Gao, J., 2015. Surface wind pressure tests on buildings with various non-uniformity morphological parameters. *J. Wind Eng. Ind. Aerodyn.* 137, 14–24.
- Mazarakis, N., Kaloudis, E., Nazos, A., Nikas, K.-S.P., 2016. LES and RANS comparison of flow and pollutant dispersion in urban environment. *Int. J. Environ. Stud.* 73 (1), 48–65.
- Mei, S.-J., Luo, Z., Zhao, F.-Y., Wang, H.-Q., 2019. Street canyon ventilation and airborne pollutant dispersion: 2-D versus 3-D CFD simulations. *Sustain. Cities Soc.* 50, 101700.
- MND, 2000. In: (MND), M.o.N.D. (Ed.), Final Report on Land Allocation. Ministry of National Development (MND), Singapore.
- Mooney, P., Dorer, V., Carmeliet, J., 2012. Effect of flow unsteadiness on the mean wind flow pattern in an idealized urban environment. *J. Wind Eng. Ind. Aerodyn.* 104–106, 389–396.
- MSS, 2011. Climate of Singapore [cited 2021 March]; Available from: <http://www.weather.gov.sg/climate-climate-of-singapore/>.
- Murena, F., Favale, G., Vardoulakis, S., Solazzo, E., 2009. Modelling dispersion of traffic pollution in a deep street canyon: application of CFD and operational models. *Atmos. Environ.* 43 (14), 2303–2311.
- NEA, 2014. In: Agency, N.E. (Ed.), Computation of the pollutant standards index (PSI). National Environment Agency (NEA), Singapore.
- NEA, 2021. Air quality in Singapore [cited 2021 March]; Available from: <https://www.nea.gov.sg/our-services/pollution-control/air-pollution/air-quality>.
- Ng, E., 2009. Policies and technical guidelines for urban planning of high-density cities—air ventilation assessment (AVA) of Hong Kong. *Build. Environ.* 44 (7), 1478–1488.
- Ng, E., Yuan, C., Chen, L., Ren, C., Fung, J.C., 2011. Improving the wind environment in high-density cities by understanding urban morphology and surface roughness: a study in Hong Kong. *Landscape Urban Plan.* 101 (1), 59–74.
- Ng, W.-Y., Chau, C.-K., 2014. A modeling investigation of the impact of street and building configurations on personal air pollutant exposure in isolated deep urban canyons. *Sci. Total Environ.* 468, 429–448.
- Oke, T.R., Street design and urban canopy layer climate. *Energy Build.*, 1988. 11(1–3): p. 103–113.
- Qian, Z., He, Q., Lin, H.-M., Kong, L., Bentley, C.M., Liu, W., Zhou, D., 2008. High temperatures enhanced acute mortality effects of ambient particle pollution in the “oven” city of Wuhan, China. *Environ. Health Perspect.* 116 (9), 1172–1178.
- Ramponi, R., Blocken, B., Laura, B., Janssen, W.D., 2015. CFD simulation of outdoor ventilation of generic urban configurations with different urban densities and equal and unequal street widths. *Build. Environ.* 92, 152–166.
- Salim, S.M., Buccolieri, R., Chan, A., Di Sabatino, S., 2011. Numerical simulation of atmospheric pollutant dispersion in an urban street canyon: comparison between RANS and LES. *J. Wind Eng. Ind. Aerodyn.* 99 (2–3), 103–113.
- Sha, C., Wang, X., Lin, Y., Fan, Y., Chen, X., Hang, J., 2018. The impact of urban open space and ‘lift-up’ building design on building intake fraction and daily pollutant exposure in idealized urban models. *Sci. Total Environ.* 633, 1314–1328.
- Shen, J., Gao, Z., Ding, W., Yu, Y., 2017. An investigation on the effect of street morphology to ambient air quality using six real-world cases. *Atmos. Environ.* 164, 85–101.
- Soulhac, L., Garbero, V., Salizzoni, P., Mejean, P., Perkins, R., 2009. Flow and dispersion in street intersections. *Atmos. Environ.* 43 (18), 2981–2996.
- Thaker, P., Gokhale, S., 2016. The impact of traffic-flow patterns on air quality in urban street canyons. *Environ. Pollut.* 208, 161–169.
- Tominaga, Y., Stathopoulos, T., 2011. CFD modeling of pollution dispersion in a street canyon: comparison between LES and RANS. *J. Wind Eng. Ind. Aerodyn.* 99 (4), 340–348.
- Tominaga, Y., Stathopoulos, T., 2013. CFD simulation of near-field pollutant dispersion in the urban environment: a review of current modeling techniques. *Atmos. Environ.* 79, 716–730.
- Tominaga, Y., Mochida, A., Yoshie, R., Kataoka, H., Nozu, T., Yoshikawa, M., Shirasawa, T., 2008. AIJ guidelines for practical applications of CFD to pedestrian wind environment around buildings. *J. Wind Eng. Ind. Aerodyn.* 96 (10–11), 1749–1761.
- Tsai, M., Chen, K., 2004. Measurements and three-dimensional modeling of air pollutant dispersion in an urban street canyon. *Atmos. Environ.* 38 (35), 5911–5924.
- URA, 2019. Draft master plan 2019 - proposals for an inclusive, sustainable and resilient city [cited 2021 March]; Available from: <https://www.ura.gov.sg/Corporate/Media-Room/Media-Releases/pr19-13>.
- URA, 2021. Master plan [cited 2021 March]; Available from: <https://www.ura.gov.sg/Corporate/Planning/Master-Plan>.
- Velasco, E., Roth, M., 2012. Review of Singapore's air quality and greenhouse gas emissions: current situation and opportunities. *J. Air Waste Manage. Assoc.* 62 (6), 625–641.
- Velasco, E., Tan, S.H., 2016. Particles exposure while sitting at bus stops of hot and humid Singapore. *Atmos. Environ.* 142, 251–263.
- Wen, C.-Y., Juan, Y.-H., Yang, A.-S., 2017. Enhancement of city breathability with half open spaces in ideal urban street canyons. *Build. Environ.* 112, 322–336.
- WHO, 2016. WHO global urban ambient air pollution database [cited 2021 March]; Available from: [https://www.who.int/phe/health\\_topics/outdoorair/databases/cities/en/](https://www.who.int/phe/health_topics/outdoorair/databases/cities/en/).
- WHO, 2021. What are the effects on health of transport-related air pollution? [cited 2021 March]; Available from: <https://www.euro.who.int/en/data-and-evidence/evidence-informed-policy-making/publications/hen-summaries-of-network-members-reports/what-are-the-effects-on-health-of-transport-related-air-pollution>.
- Xie, X., Huang, Z., Wang, J.-s., 2005. Impact of building configuration on air quality in street canyon. *Atmos. Environ.* 39 (25), 4519–4530.

- Yim, S.H., Fung, J.C.H., Lau, A.K.-H., Kot, S.C., 2009. Air ventilation impacts of the “wall effect” resulting from the alignment of high-rise buildings. *Atmos. Environ.* 43 (32), 4982–4994.
- Yuan, C., Ng, E., Norford, L.K., 2014. Improving air quality in high-density cities by understanding the relationship between air pollutant dispersion and urban morphologies. *Build. Environ.* 71, 245–258.
- Zhang, K., Batterman, S., 2013. Air pollution and health risks due to vehicle traffic. *Sci. Total Environ.* 450, 307–316.